The Effect of Nano-SiO₂ on the Structural, Electrical and Magnetic Properties of SiO₂-LiFe₅O₈ Glass–ceramics Prepared by Sol Gel Auto-combustion Processing

N.M. Shash[1], M.M. Rashad[2,*], M.G. El-Shaarawy[1], M.H. Maklad[2] , F.A. Afifi[3]

[1] *Physics Department, Faculty of Science, Benha University, Benha, Egypt*
[2] *Central Metallurgical Research and Development Institute (CMRDI), Helwan, Cairo, Egypt*
[3] *Basic Engineering Science Department, Faculty of Engineering, Benha University, Benha, Egypt*

The glass–ceramic with the composition x(LiFe₅O₈)/(100 − x) SiO₂ (x = 20, 30, 40, 50, 100 wt. %) were prepared by sol gel auto-combustion method. The influence of the SiO2 ratio in the glass-ceramics strucure prepared was investigated by X-ray diffraction (XRD) and scanning electron microscopy (SEM). Crystalline phases (LiFe₅O₈, SiO₂, Fe₂O₃) were observed by X-ray powder diffraction in the glasses annealed at 800 °C for 2h. The crystallite size was found to increase from 27.29 nm (x = 20%) to 91.48 nm (x = 100 %). The microstructure of the formed powders was SiO₂ ratio dependent. Increasing the SiO₂ ratio was found to inhibit the grain growth of the formed ferrite. The electrical conductivity of glass-ceramics samples were raised with increasing the concentration of SiO₂ ratio as the result of increasing the hopping of electrons between Fe^{2+} and Fe^{3+} ions. The magnetic characteristics of the prepared glass ceramics were performed using a vibrating sample magnetometer in function of the magnetic field. The samples heat-treated at 800 °C for 2h present a ferrimagnetic behavior. Alongside, the formed crystalline silicate lithium ferrite had good magnetic properties. High saturation magnetization (51.9 emu/g) was attained the formed ferrite sample of x = 100 % ratio annealed at 800°C for 2h.

Keywords: Spinel ferrite, Combustion synthesis, Microstructure, Electrical properties, Magnetic properties.

PACS numbers: 81.20.Fw, 75.75.+a

1. INTRODUCTION

The preparation of LiFe₅O₈ nanoparticles embedded in a glass matrix, through the sol-gel method is a topic with a few numbers of published works. The sol-gel method shows considerable advantages relatively to the conventional methods because it allows preparing new glass and glass–ceramic compositions, at low temperatures and permit, through heat-treatments, control the size and morphology of the crystallized particles [1]. The effect of on nano-SiO₂ various structural, microstructure, electrical, dielectric and magnetic properties has been reported, and a mutual influence between the structure and the cationic distribution is recognized. It seems only very little work has been done so far on the cation distribution of silicate lithium ferrites [2]. Therefore, in the present work, we focused on the synthesis of silicate lithium ferrite using sol gel auto-combustion method using urea as a fuel. Our previous studied involved that the existence of pure lithium ferrite with good magnetic properties was obtained using urea based on sol gel reaction method at different calcined temperatures from 400 to 800 °C for 2h. Hence, the impact of SiO₂ ratio on the crystal structure, microstructure, conductivity and magnetic properties of the new synthesized x (LiFe₅O₈)/(100 − x) SiO₂ nanoparticles with (x = 20, 30, 40, 50, 100 wt. %) is extensively studied using different physical approaches in this work.

Recent developments of lithium ferrite have attracted a lot of research interest due to advantageous properties such as high saturation magnetization, low dielectric losses and excellent square shaped of hysteresis curve, excellent dielectric properties, high resistivity ~ $10^8 \Omega$ cm, lower eddy current, relatively high Curie temperature (620 ℃), high chemical inertness, thermal stability, high resistivity and low eddy current losses, low cost and safety. Due to these unique properties, it promises to be a potential prolonged application for microwave devices instead of expensive yttrium iron garnet (YIG) like circulators, phase shifters, isolators, power transformation in electronics, memory core, antennas and high-speed digital tapes. Furthermore, it is exploited for lithium ion batteries, high-density magnetic recording, magnetic fluids, magneto-caloric refrigeration, magnetic resonance imaging enhancement, magnetically guided drug delivery and multilayer chips inductors [3]. Numerous wet chemical methods have been applied to synthesize lithium ferrite fine particles including ball milling [4], sol gel [5], combustion method [6-8], hydrothermal [5,10-11], solvothermal [12], aerosol route [13] co-precipitation [14] and microemulsion [9] techniques. It is claim mentioning that ferrites powders prepared by sol gel auto-combustion method technique at low annealing temperature possesses homogeneous microstructure, fine particle size, narrow size distribution, minimum particle agglomeration good chemical purity and improved physical properties [10-18]. Meanwhile, the origin of magnetic and dielectric properties of lithium ferrite is regarded to the variety of metal substitution.

2. EXPERIMENTAL PROCEDURE

The glass–ceramics samples of the composition x (LiFe₅O₈)/(100 − x) SiO₂ (x = 20, 30, 40, 50, 100 wt. %) have been synthesized using sol gel auto-combustion method based on urea as a fuel. Chemically grade ferric nitrate (Fe(NO₃)₃ · 9H₂O), lithium nitrate (Li-

$NO_3.3H_2O$), (TEOS) tetraethylorthosilicate ($C_8H_{20}O_4Si$) [M.W 208.32 with purity 99%] and urea ($NH_2.CO\ NH_2$) were used as starting materials as shown in Fig. 1. The aqueous solution of ferric, lithium and TEOS with Fe^{3+}: Li^+ molar ratios (1.5) to x ($LiFe_5O_8$)/(100 − x) SiO_2 [19] was gently stirred on hot-plate magnetic stirrer for 15 min. followed with addition of an aqueous solution of urea to the mixtures with continuous stirring. The pH of the solution was adjusted at 7 by adding ammonia solution to form the gel. The solution was evaporated to 80 °C with constant stirring until viscous resin was formed and then dried at 100°C overnight. For the formation of the silicate lithium ferrite phase, the dry precursors of x ($LiFe_5O_8$)/(100 − x) SiO_2 (x = 20, 30, 40, 50, 100 wt. %) were annealed at the rate of 10 °C/min in static air atmosphere at 800 °C and maintained at the temperature for annealed time 2 h. The measurements were carried out in a current of argon atmosphere. The crystalline phases presented in the different annealed samples were distinguished by X-ray diffraction XRD on a Brucker axis D8 diffractometer using Cu-Kα (λ = 1.5406 Å) radiation and secondary monochromator in the range 2θ from 20 to 70°. The change in ferrites particles morphologies was adjusted by field emission scanning electron microscope (FE-SEM, QUANTA FEG 250). The ac electrical conductivity for the investigated samples was performed over a temperature range from 30 to 200°C and frequency range from 20Hz to 10MHz using (LCR-8110G) precision LCR meter. The magnetic properties of the ferrites were measured at room temperature using a vibrating sample magnetometer (400-1 VSM, U.S., Lake Shore Co., Ltd., USA) in a maximum applied field of 20 kOe. From the obtained hysteresis loops, the saturation magnetization (M_s), remanence magnetization (M_r) and coercivity (H_c) were determined.

3. RESULTS AND DISCUSSION

3.1 Crystal structure

Fig. 2 shows the powder X-ray diffraction patterns of x ($LiFe_5O_8$)/(100 − x) SiO_2 (x = 20, 30, 40, 50, 100 wt.%) powders synthesized by sol-gel auto combustion using urea annealed at 800 °C for 2h. It was evident that the silicate lithium ferrite specimens contain crystalline
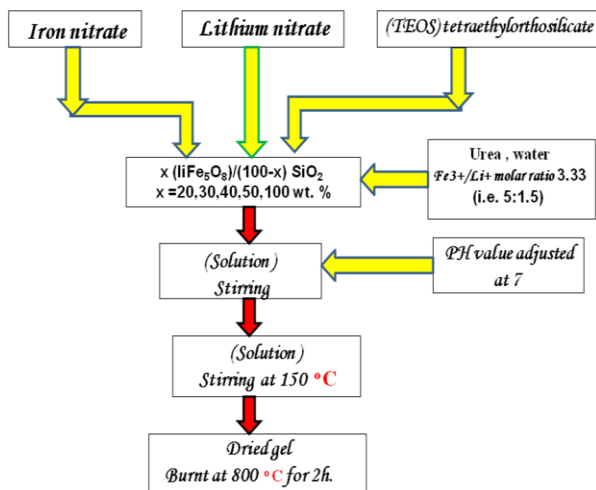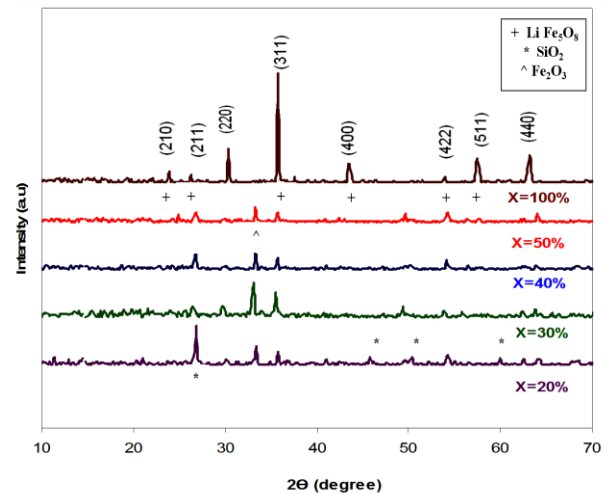

Fig. 2 – XRD patterns of x ($LiFe_5O_8$)/(100 − x) SiO_2 (x = 20, 30, 40, 50, 100 wt. %) powders annealed at 800 °C for 2h.

phases ($LiFe_5O_8$, SiO_2, Fe_2O_3) which observed by X-ray powder diffraction in the glasses annealed at 800 °C for 2h. The influence of the SiO_2 ratio in the glass-ceramics structure prepared was investigated by X-ray diffraction (XRD). The diffraction pattern of the x = 100 % sample was exhibited well crystalline cubic $LiFe_5O_8$ (JCPDS # 82-1436) phase. The diffraction peaks belonging to (210) (211) (220) (311) (400) (422) (511) and (400) planes of lithium ferrite were indexed.

Noticeably, lattice parameter (a) as well as unit cell volume (V_{cell}) of the silicate lithium ferrite specimens was calculated and the results were listed in Table 1. The measured lattice parameter for x ($LiFe_5O_8$)/(100 − x) SiO_2 phase was found to be 0.833 ± 0.01 nm which was in good agreement with that mentioned in the JCPDS card. Alongside, Table 1 also records the crystallite sizes of x ($LiFe_5O_8$)/(100 − x) SiO_2 ferrites for the most intense peak [(3 1 1) plane] observed at $2\theta \approx 35.825°$ based on the XRD data using the Debye-Scherrer formula. It was found that the crystallite size was minified with addition of SiO_2 ratio. It was found to reduce from 91.5 nm for pure lithium ferrite (x = 100%) to 27.29 nm for (x = 20 %).

Table 1 – Average crystallite size, lattice constant and cell volume for x ($LiFe_5O_8$)/(100 − x) SiO_2 ferrite samples annealed at 800 °C for 2h.

X (wt. %)	Average crystallite size(nm)	Lattice constant (°A)	Cell volume (°A³)
20	27.296	8.513	616.867
30	36.399	8.516	617.499
40	39.951	8.526	619.696
50	51.187	8.502	614.498
100	91.482	8.307	573.219

3.2 Microstructure

Fig. 3 displays the field emission scanning electron microscope (FE-SEM) of x ($LiFe_5O_8$)/(100 − x) SiO_2 (x = 20, 30, 40, 50, 100 wt.%) powders annealed at 800 °C for 2h.

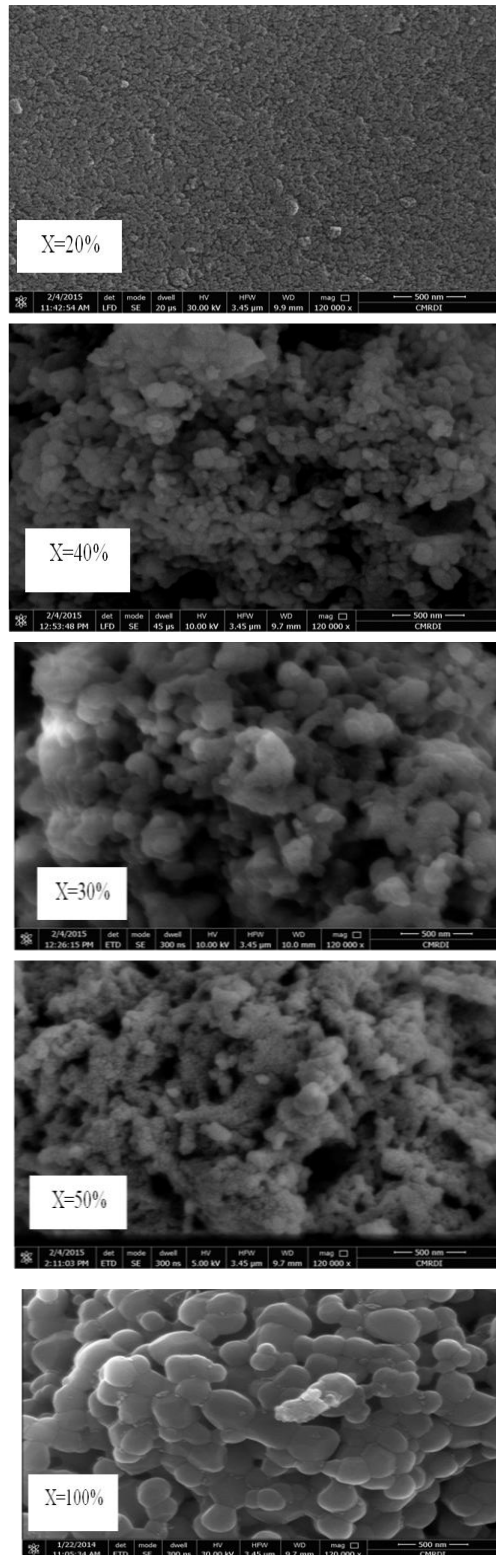**Fig. 1** – Flow chart of silicate lithium ferrite sol-gel procedure.

Fig. 3 – SEM images of x (LiFe$_5$O$_8$)/(100 − x) SiO$_2$ powders annealed at 800 °C for 2h.

It is clear that the distribution of the grains with uniform size in each composition was observed. Besides, the grain size was significantly depended on the SiO$_2$ ratio. The grain size was gradually minimized with increasing SiO$_2$ content which agrees with XRD results.

3.3 Electrical properties

3.3.1 The Temperature dependence of AC conductivity

Fig. 4 illustrates the temperature dependence of AC conductivity, σ_{ac}, for all investigated samples of x (LiFe$_5$O$_8$)/(100 − x) SiO$_2$ (x = 20, 30, 40, 50, 100 wt.%) powders annealed at 800 °C for 2h over a temperature range from 30 to 200°C and frequency range from 20Hz
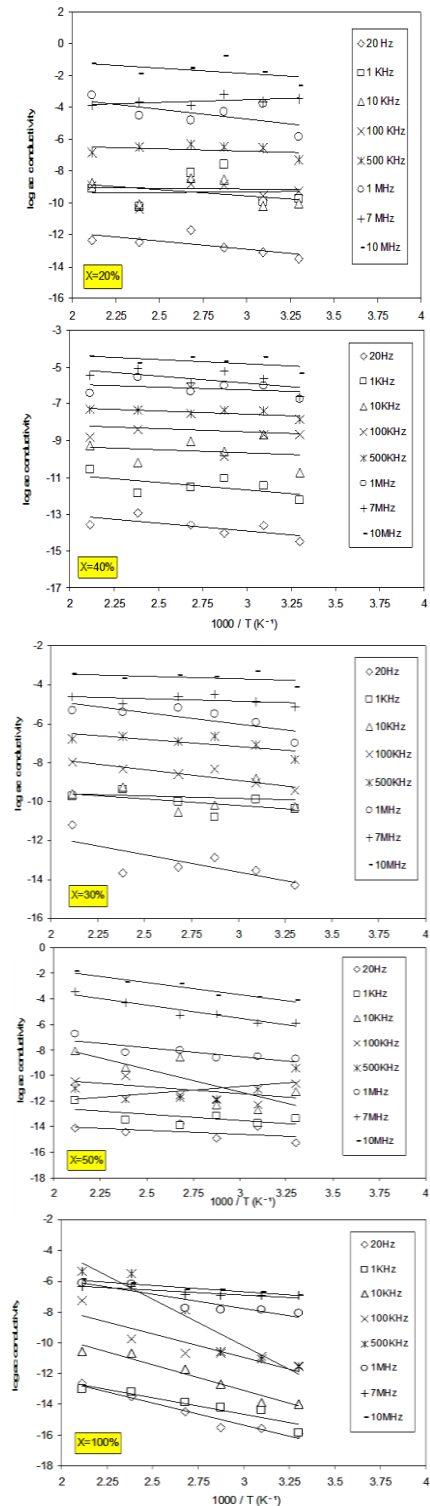

Fig. 4 – Electrical conductivity versus inverse of temperatures for x (LiFe$_5$O$_8$)/(100 − x) SiO$_2$ powders annealed at 800 °C for 2h.

to 10MHz. The relation between the temperature and AC conductivity σac was estimated from the Arrhenius expression as the following:

$$\sigma_{ac} = \sigma_0 \exp(-E_{a(ac)}/kT) \qquad (3.1)$$

Where σ_0 is the pre- exponential factor contains several constants, k is the Boltzmann's constant, T is the absolute temperature and $E_{a(ac)}$ is the AC activation energy for conduction.

The activation energies were calculated from straight line fit using Eq. 3.1 compositions and they were given in Table 2. It is noticeable that the AC conductivity σ_{ac} was steadily increased upon increasing of temperature and SiO₂ content. However, the mechanism of electrical conduction is similar to that of dielectric polarization. In the low frequency region, grain boundaries with high resistance were effective, giving a constant plateau region (σ_{ac}). At higher frequencies, the increase in conductivity was imputed to grain effect and increased hopping of charge carriers between Fe^{2+}/Fe^{3+} ions at the adjacent octahedral sites [19, 20]. On the other hand, the increase in conductivity with temperature was related to thermally activated hopping of charge carriers [21, 22]. Additionally, the increment of σ_{ac} with SiO₂ ratio was attributed to the increase in the magnitude of electronic exchange which was dependent on the concentration of Fe3+/Fe2+ ion pairs present on B-site as depicted in Fig. 5.

Table 2 – Activation energies obtained from Arrhenius plots for x (LiFe₅O₈)/(100 − x) SiO₂ powders annealed at 800 °C for 2h.

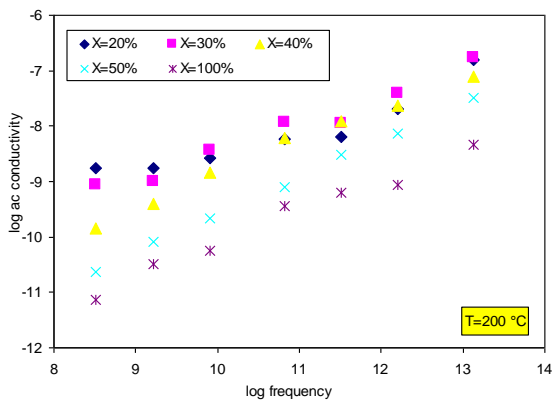| x (wt. %)	$E_{a(ac)}$(eV)							
	20Hz	1KHz	10KHz	100KHz	500KHz	1MHz	7MHz	10MHz
20	0.086	0.007	0.067	0.007	0.024	0.108	0.028	0.002
30	0.155	0.058	0.023	0.095	0.063	0.102	0.022	0.002
40	0.072	0.069	0.030	0.028	0.029	0.027	0.067	0.006
50	0.054	0.082	0.305	0.093	0.097	0.120	0.178	0.015
100	0.300	0.172	0.168	0.189	0.215	0.330	0.203	0.017

Fig. 5 – Dependence of ac electrical conductivity on x ratio of x (LiFe₅O₈)/(100 − x) SiO₂ powders annealed at 800 °C for 2h.

3.3.2 The Frequency dependence of ac conductivity

Generally, the total conductivity is expressed by the following power relation

$$\sigma_{ac}(\omega) = A\cdot\omega^s \qquad (3.2)$$

Where A is a temperature dependent parameter, ω is the angular frequency and the frequency exponent s is a temperature-dependent parameter with values between 0 and 1. Fig. 6 presents the variation of electrical conductivity $\sigma_{ac}(\omega)$ with frequency 20 Hz to 10 MHz. One can note that values of conductivity were gradually increased with increasing the applied field frequency. The increasing in (σ_{ac}) with applied field frequency was explicated in the fact that the pumping force of the applied frequency that helps in transferring the charge carriers between the different localized states as well as liberating the trapped charges from the different trapping centers. The exponent s was determined as a function of composition for each sample, in the temperature range from 30 to 200 °C by plotting ln σ versus ln ω according to Eq. 2 as depicted in Fig. 6 which represents straight lines with slope equal to the exponent s and the variation of the exponent s is given in Table 3. It is obviously that the value of s was between 0 and 1. When $s = 0$, the electrical conduction was frequency independent or DC conduction, but for $s \le 1$, the conduction was frequency dependent or AC conduction. Consequently, it is distinctly that the exponent s was located in two ranges. In the range $0.5 \le s \le 1$ which evidenced the electron hopping between Fe^{+2} and Fe^{+3} ions and the values of $s \le 0.5$ which demonstrated the domination of ionic conductivity [23]. Table 3 devotes the values of s which proved that the exponent s was positioned in the two ranges. Therefore, the manner of σ′ with frequency and s with temperature denoted that the classical barrier hopping model is the most favorable mechanism to expound the conduction mechanism for the compositions under investigation. The charge carriers responsible for the conduction process are the electron hopping between Fe^{2+} and Fe^{3+} ions in the case of silicate lithium ferrite samples.

Table 3 – The values of the exponent "s value" for x (LiFe₅O₈)/(100 − x) SiO₂ powders annealed at 800 °C for 2h.at different temperatures.

x (wt. %)	s value					
	30 °C	50 °C	75 °C	100 °C	150 °C	200 °C
20	0.291	0.222	0.294	0.479	0.408	0.393
30	0.527	0.575	0.591	0.613	0.524	0.495
40	0.474	0.369	0.422	0.243	0.287	0.284
50	0.499	0.489	0.397	0.515	0.417	0.562
100	0.692	0.648	0.831	0.998	0.874	0.855

3.4 Magnetic properties

The magnetization of x (LiFe₅O₈)/(100 − x) SiO₂ powders was measured at room temperature under an applied field of 20 kOe and the hysteresis loops of the ferrite
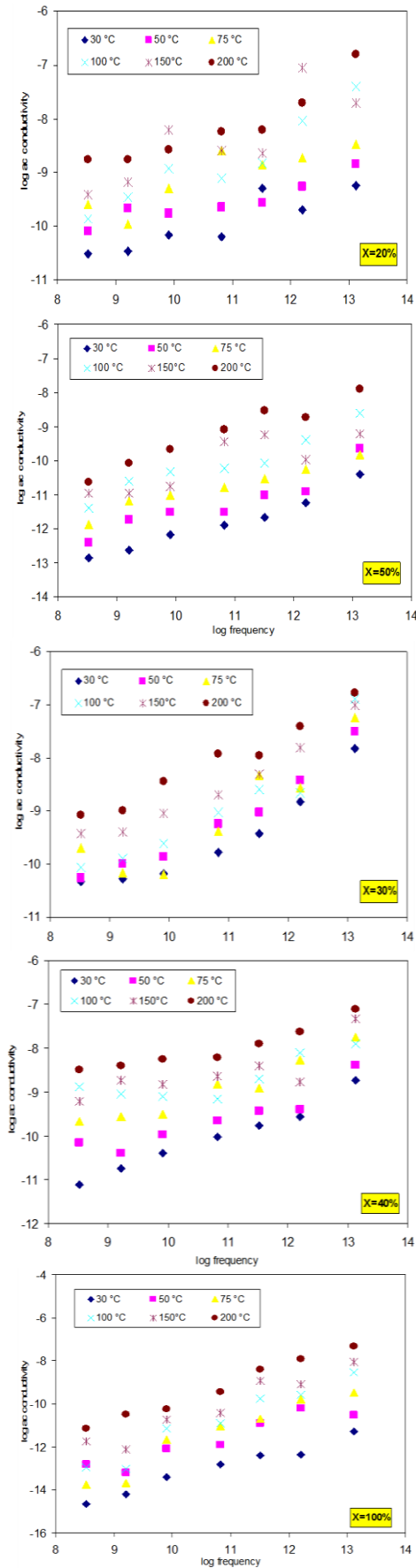
powders were obtained. Fig. 7 shows the nexus of magnetization (M) as a function of applied field (H). Subsequently, the magnetic parameters are listed in Table 4. It is distinctly that the saturation magnetization of the ferrite powders was increased with increasing the x content upon $x = 40 \%$. Thereafter, it was decreased with $x = 50\%$. The observed magnetization was a result of the simultaneous influence of several extrinsic and intrinsic factors such as density, anisotropy, grain size, cation distribution and the A–B exchange interaction [24-25]. With further incorporation of x content ($x > 50 \%$), the increase in M_s can be attributed to the increased migration of Fe^{3+} ions from the A- to B-site. This migration results in an increase in Fe^{3+} ion concentration at B-site which gives rise to parallel spin coupling. This results in the strong of the A–B exchange interaction, leading to the increasing of the magnetization [26-30]. Moreover anomalous behavior of H_c was due to the different magnetic moment of Fe in silica. This may be imputed to changes in the particle size and the low magnetic anisotropy [31-34].

Table 4 – The magnetic properties for x $(LiFe_5O_8)/(100 - x)$ SiO_2 ferrite samples annealed at 800 °C for 2h.

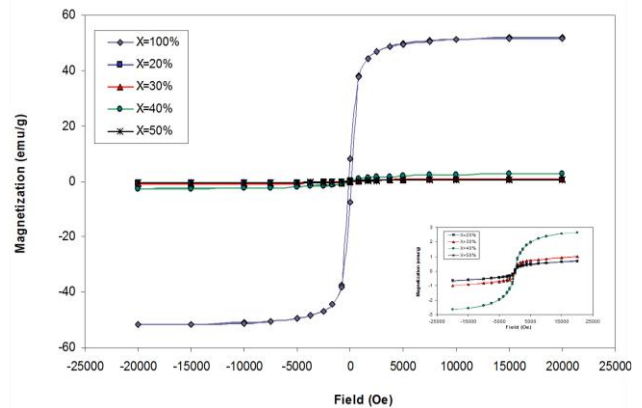| x (wt. %)	M_s (emu/g)	M_r(emu/g)	Hc (Oe)
20	0.665	0.069	194.70
30	1.000	0.123	244.23
40	2.634	0.100	96.161
50	0.712	0.075	221.03
100	51.896	7.960	145.72

Fig. 7 – M-H hysteresis loop of of x $(LiFe_5O_8)/(100 - x)$ SiO_2 powders annealed at 800 °C for 2h.

4. CONCLUSIONS

The glass-ceramic with the composition x $(LiFe_5O_8)/(100 - x)$ SiO_2 nanopowders have been successfully synthesized by sol gel auto-combustion method using urea as an organic fuel. The results from XRD, FE-SEM, AC electrical conductivity and VSM studies are summarized as follows:

- The crystallite size was found to increase from 27.29 nm ($x = 20 \%$) to 91.48 nm ($x = 100 \%$).
- Crystalline phases of ($LiFe_5O_8$, SiO_2, Fe_2O_3) were observed by XRD analysis.
- The crystallite size of the formed powders was found to minify with increasing the SiO_2 content. It was found to decrease from 91.5 nm for pure lithi-

Fig. 6 – Dependence of AC conductivity on the frequency of x $(LiFe_5O_8)/(100 - x)$ SiO_2 powders annealed at 800 °C for 2h.

um ferrite to 27.3 nm with SiO_2 ratio of 80 %.

- The microstructure of x $(LiFe_5O_8)/(100-x)$ SiO_2 powders was dependent on content of SiO_2.
- AC conductivity of the formed ferrite powders was slightly increased at low frequencies and abruptly at high frequencies. Moreover, Ac conductivities of these ferrites were increased as the result of the increment of temperature and content of SiO_2 due to increase the hopping of electrons between Fe^{2+} and Fe^{3+} ions.
- The formed glass-ceramic with the composition x $(LiFe_5O_8)/(100-x)$ SiO_2 powders had good magnetic properties. High saturation magnetization (51.9 emu/g) was fulfilled for the formed ferrite at anneal-

ing temperature 800 °C for 2h with $x = 100$ %.

- Such ferrite nanomaterials would be good candidate for several potential applications including, e.g. microwave devices and high-density magnetic recording media. These ferrite compositions are useful for the multilayer chip inductors which are important components for electronic products such as notebook computer and cellular phone.

ACKNOWLEDGMENTS

REFERENCES

1. M.M. Rashad, M.G. El-Shaarawy, N.M. Shash, M.H. Maklad, F.A. Afifi, *J. Magn. Magn. Mater.* **374**, 495 (2015).
2. Dipti P. Kumar, J.K. Juneja, S. Singh, K.K. Raina, C. Praksah, *Ceram. Inter.* **41**, 3293 (2015).
3. M. Srivastava, S. Layek, J. Singh, A.K. Das, H.C. Verma, A.K. Ojha, N.H. Kim, J.H. Lee, *J. Alloys Compd.* **591**, 174 (2014).
4. S.A. Mazen, N.A. Abu-Saad, *Appl. Nanosci.* **5**, 105 (2015).
5. H. Zeng, T. Tao, Y. Wu, W. Qi, C. Kuang, S. Zhou, Y. Chen, *RSC Advances* **4**, 23145 (2015).
6. P.V.B. Reddy, B. Ramesh, Ch. G. Reddy, *Physica B* **405**, 1852 (2010).
7. A. Sutka, G. Mezinskis, *Front. Mater. Sci.* **6**, 128 (2012).
8. R.P. Patil, B.V. Jadhav, P.P. Hankare, *Res. Phys.* **3**, 214 (2013).
9. V.S. Sawant, K.Y. Rajpure, *J. Magn. Magn. Mater.* **382**, 152 (2015).
10. X. Wang, L. Gao, L. Li, H. Zheng, Z. Zhang, W. Yu and Y. Qian, *Nanotechnology* **16**, 2677 (2005).
11. H. Zeng, T. Tao, Y. Wu, W. Qi, C. Kuang, S. Zhouand, Y. Chen, *RSC Advances* **4**, 23145 (2014).
12. B. Li, Y. Xie, H. Su, Y. Qian, X. Liu, *Solid State Ionics* **120**, 251 (1999).
13. S. Singhal, K. Chandra, *J. Electromagnetic Applications & Analysis* **2**, 51 (2010).
14. M. A. Dar, J. Shah, W.A. Siddiqui, R.K. Kotnala, *J. Alloys Compd.* **523**, 36 (2012).
15. M. Rasly, M. M. Rashad, *J. Magn. Magn. Mater.* **337-338**, 58 (2013).
16. M.M. Rashad, A.O. Turky, A.T. Kandil, *J. Mater. Sci. Mater. Electron.* **24**, 3284 (2013).
17. M.M. Rashad, *J. Mater. Sci. Mater. Electron.* **23**, 882 (2012).
18. M.M Rashad, M.G. Fayed, T.M. Sami, E.E. El-Shereafy, *J. Mater. Sci. Mater. Electron.* **26**, 1259 (2015).
19. G. Aravind, M. Raghasudha, D. Ravinder, *J. Magn. Magn. Mater.* **378**, 152 (2015).
20. Viswarupa Mohanty, Rajesh Cheruku, Lakshmi Vijayan, G. Govindaraj, *J. Mater. Sci. Technol.* **30**, 335 (2014).
21. S.A. Mazen, N.I. Abu-Elsaad, *Ceram. Inter.* **40**, 11229 (2014).
22. P.R. Arjunwadkar, R.R. Patil, *J. Alloys Compd.* **611**, 273 (2014).
23. B.K. Kuanr, G.P. Srivastava, *J. Appl. Phys.* **75**, 6115 (1994).
24. T. Namgyal, J. Singh, K. Chandra, S. Bansal, S. Singhal, *J. Molecular Structure* **1019**, 103 (2012).
25. M.J. Iqbal, M.I. Haider, *Mater. Chem. Phys.* **140**, 42 (2013).
26. M. Ramesh, G. S. N. Rao, K. Samatha, B. P. Rao, *Ceram. Inter.* **41**, 1765 (2015).
27. S.K. Gurav, S.E. Shirsath, R.H. Kadam, S. M. Patange, K.S. Lohar, D.R. Mane, *Mater. Res. Bull.* **48**, 3530 (2013).
28. Y.-P. Fu, S.-H. Hu, *Ceram. Inter.* **36**, 1311 (2010).
29. M.A. Dar, K.M. Batoo, V. Verma, W.A. Siddiqui, R.K. Kotnala, *J. Alloys Compd.* 493, 553 (2010).
30. A.A. Kadam, S.S. Shinde, S.P. Yadav, P.S. Patil, K.Y. Rajpure, J. Magn. Magn. Mater. **329**, 59 (2013).
31. R. Cheruku, G. Govindaraj, L. Vijayan, *Mater. Chem. Phys.* **146**, 389 (2014).
32. S.S. Teixeira, M.P.F. Graça, L.C. Costa, M.A. Valente, *Mater. Sci. Eng: B* **186**, 83 (2014).
33. S.I. Hussein, A.S. Elkady, M.M. Rashad, A.G. Mostafa, R.M. Megahid, *J. Magn. Magn. Mater.* **379**, 9 (2015).
34. M.M. Rashad, M.I. Nasr, *Electron. Mater. Lett.* **8**, 325 (2012).